Stem Cell Reports, Volume *12*

Supplemental Information

Human iPSC-Derived Retinas Recapitulate the Fetal CRB1 CRB2 Complex Formation and Demonstrate that Photoreceptors and Müller Glia Are Targets of AAV5

Peter M. Quinn, Thilo M. Buck, Aat A. Mulder, Charlotte Ohonin, C. Henrique Alves, Rogier M. Vos, Monika Bialecka, Tessa van Herwaarden, Elon H.C. van Dijk, Mays Talib, Christian Freund, Harald M.M. Mikkers, Rob C. Hoeben, Marie-José Goumans, Camiel J.F. Boon, Abraham J. Koster, Susana M. Chuva de Sousa Lopes, Carolina R. Jost, and Jan Wijnholds

Supplemental Figures and Legends

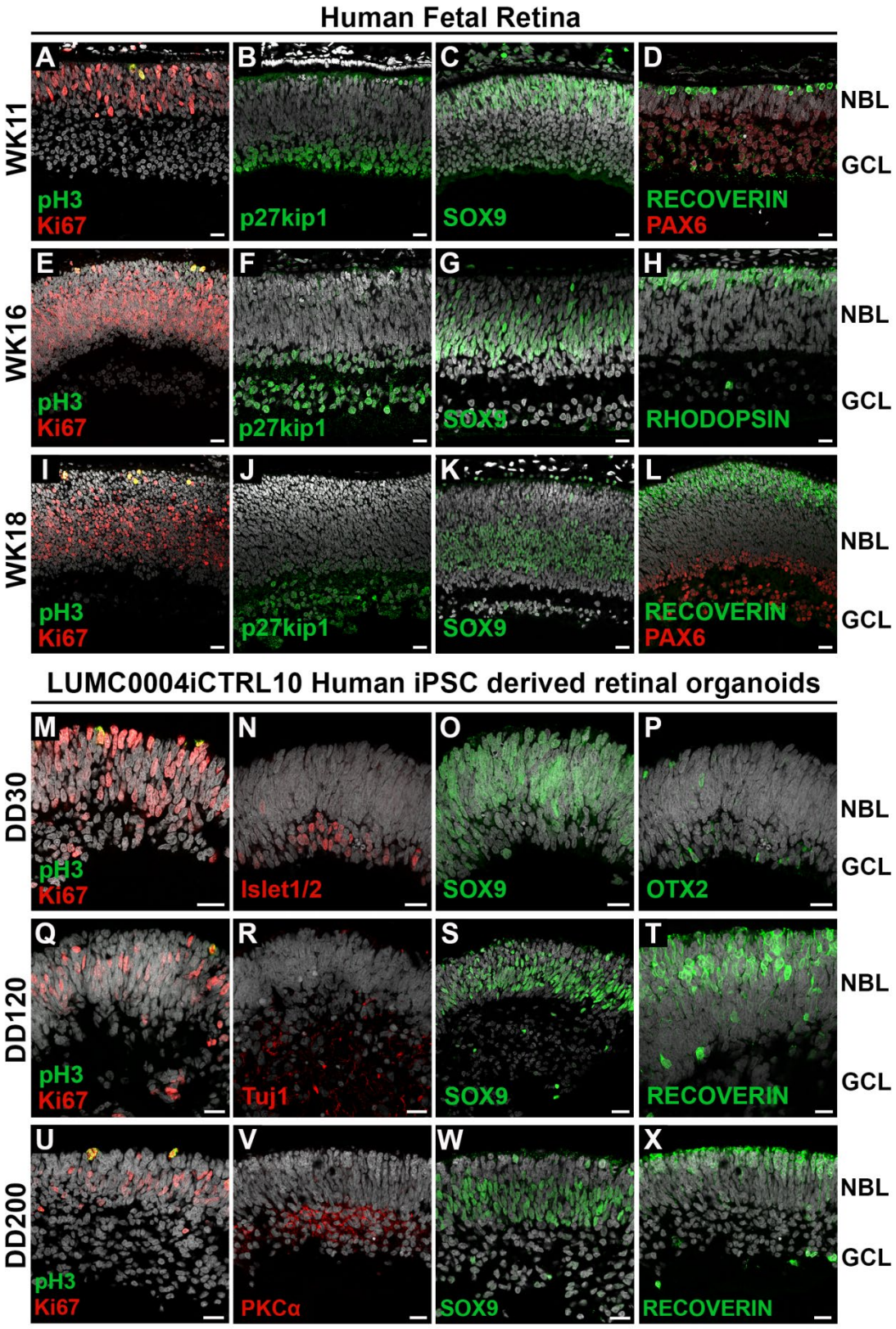

Figure S1. Retinal architecture in the human fetal retina and human iPSC retinal organoids. Related to Figure 1. Immunohistochemistry pictures of WK11 (A-D), WK16 (E-H) and WK18 (I-L) human fetal retina

and DD30 (M-P), DD120 (Q-T) and D200 (U-X) LUMC0004iCTRL10 hiPSC-derived retinal organoids. Sections were stained with antibodies against: Ki67 (A, E, I, M, Q, U), pH3 (A, E, I, M, Q, U), $p27^{kip1}$ (B, F, J), SOX9 (C, G, K, O, S, W), Recoverin (D, L, T, X), PAX6 (D, L), Rhodopsin (H), Islet1/2 (N), Tuj1 (R), PKCα (V), OTX2 (P). In human fetal retina at week 11 in the 1st trimester of pregnancy we observed cycling cells that stained positive for anti-Ki67 and spanned the thickness of the neuroblast layer (NBL). The mitotic cells located most apically and stained positive for pH3 (A). Inner retinal cells as marked by p27kip1 and PAX6 were restricted to the ganglion cell layer and a subset of cells in the NBL (B and D). The cells that exited the cell cycle were marked with p27kip1, whereas the ganglion cells, amacrine cells and migrating retinal progenitors were marked with PAX6. Radial glial progenitor cell nuclei spanned the thickness of the NBL and stained positive for anti-SOX9 (C). Newborn cone photoreceptors marked positive for anti-recoverin (D (See also Figure S2A and S2B)). In the human fetal retina at weeks 16 and 18 in the 2nd trimester of pregnancy, we observed the localisation of anti-pH3-positive mitotic cells most apically within the NBL (E and I). However, the cycling anti-Ki67-positive cells became mostly restricted to the middle NBL cells but also labelled occasional outer NBL cells (E and I). Both p27kip1- and PAX6-positive cells restricted to the inner NBL and the ganglion cell layer (F, J, L). SOX9-positive cell nuclei localised in the middle NBL and occasionally the outer NBL, marking at this stage of development both the maturing Müller glial cells and radial glial progenitor cells (G (See also Figure S2C)). The outer NBL showed an increase in recoverin-positive photoreceptors at weeks 16 and 18 compared to week 11 (H and L). Rhodopsin-positive staining indicated the presence of rod photoreceptors whose basal processes extended from the outer NBL to the bottom of the inner NBL (H). In early DD30 hiPSC retinal organoids we observed that Ki67-positive cycling cells spanned the thickness of the NBL with pH3-positive mitotic cells located most apically (M). Ki67-positive cycling cells were also detected in the ganglion cell layer (GCL). Islet1/2-positive cells were found mostly restricted to the GCL with sporadic cells in the NBL (Figure 1N). SOX9-positive radial glial progenitor cell nuclei spanned the thickness of the NBL but were also seen occasionally in the GCL (Figure 1O). Immature photoreceptors that stained positive for anti-OTX2 could be found in both the NBL and GCL (Figure 1P). In later DD120 and DD200 hiPSC-derived retinal organoids Ki67-positive cycling cells restricted mostly to the middle NBL but occasionally were detected in the outer NBL and in the GCL, whereas pH3-positive mitotic cells located apically (Q and U). In the inner retina Tuj1-positive ganglion cell axons (R) and PKCα-positive bipolar cells (V) were detected. SOX9-positive cell nuclei became more restricted to the middle NBL but occasionally were detected in the outer NBL and the GCL (S and W (See also Figure S2D)). Recoverin-positive photoreceptor cells were mostly restricted to the outer NBL. Some recoverin-positive cells were detected within the NBL and occasional recoverin-positive cells were detected in the GCL (T and X). At least two independent differentiations/samples were analysed, 3-6 sections examined per organoid or fetal eye. Scale bars: (A-X), 20μm.

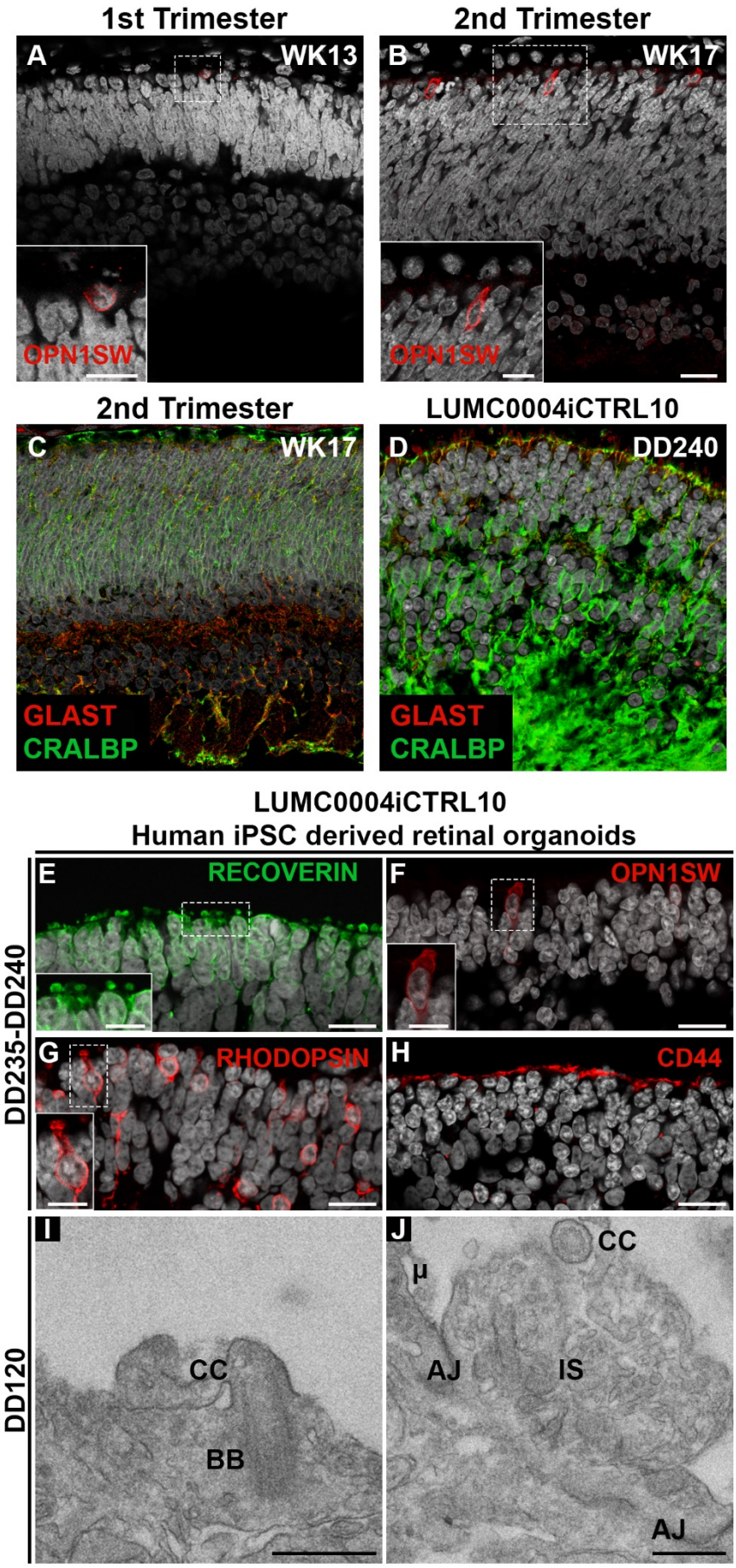
1st Trimester
2nd Trimester
A
WK13
OPN1SW
B
WK17
OPN1SW
2nd Trimester
LUMC0004iCTRL10
C
WK17
GLAST
CRALBP
D
DD240
GLAST
CRALBP
LUMC0004iCTRL10
Human iPSC derived retinal organoids
DD235-DD240
E
RECOVERIN
F
OPN1SW
G
RHODOPSIN
H
CD44
DD120
I
CC
BB
J
CC
μ
AJ
IS
AJ

Figure S2. Long-term maturation of fetal retinas and human iPSC retinal organoids. Related to Figures 1 and S1. Immunohistochemistry pictures of 1st and 2nd trimester fetal retina (A-C) and LUMC0004iCTRL10 human iPSC-derived retinal organoids (D-J). Sections were stained for OPN1SW (A, B, F), RLBP1 and GLAST (C, D), Recoverin (E), Rhodopsin (G), and CD44 (H). Human fetal retina had cones in the 1st (A) and 2nd trimester (B) and Müller glial cells in the 2nd trimester (D). Immature photoreceptor segments were detected in human iPSC retinal organoid (E) with the presence of both cones (F) and rods (G). Additionally, staining of CRALBP, GLAST and CD44 suggested the presence of Müller glial cells (D, H). Electron microscopy at DD120 confirmed a number of retinal structures including: basal bodies (I), connecting cilium (I,J), inner segment (J), adherens junction (J), microvilli (J). At least two independent differentiations/samples were analysed, 3-6 sections examined per organoid or fetal eye. CC =connecting cilium; IS = inner segment; BB =basal body; AJ adherens junction; µ= microvilli. Scale bars: (A-H), 20µm; inserts (A, B, E, F, G) 10 µm, (I, J) 500nm.

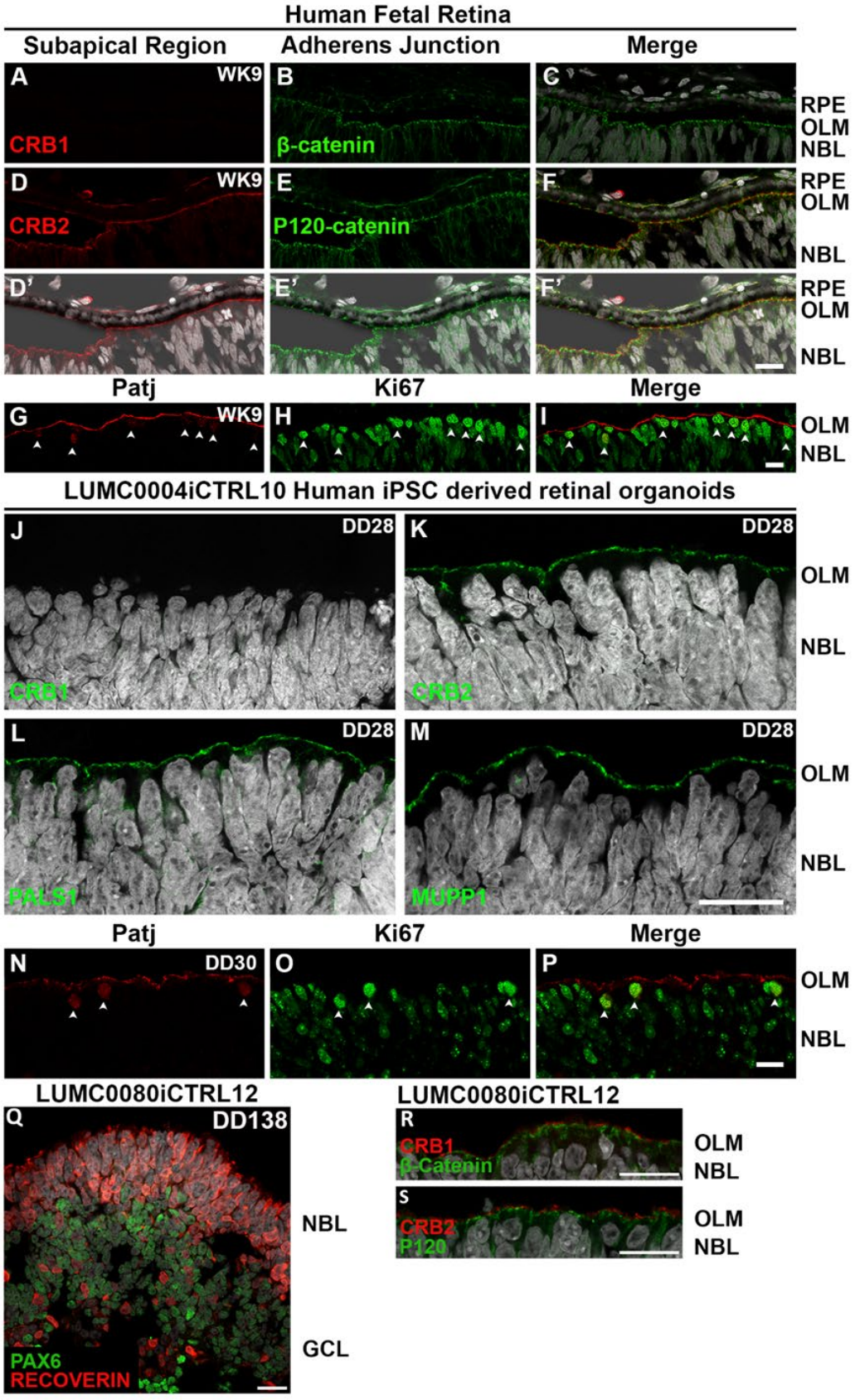
Human Fetal Retina
Subapical Region
Adherens Junction
Merge
A
WK9
CRB1
B
β-catenin
C
RPE
OLM
NBL
D
WK9
CRB2
E
P120-catenin
F
RPE
OLM
NBL
D'
E'
F'
RPE
OLM
NBL
Patj
Ki67
Merge
G
WK9
H
I
OLM
NBL
LUMC0004iCTRL10 Human iPSC derived retinal organoids
J
DD28
CRB1
K
DD28
CRB2
OLM
NBL
L
DD28
PALS1
M
DD28
MUPP1
OLM
NBL
Patj
Ki67
Merge
N
DD30
O
P
OLM
NBL
LUMC0080iCTRL12
Q
DD138
PAX6
RECOVERIN
NBL
GCL
LUMC0080iCTRL12
R
CRB1
β-Catenin
S
CRB2
P120
OLM
NBL
OLM
NBL

Figure S3. Localisation of CRB complex in the 1st trimester fetal retina and early and late human iPSC retinal organoids. Related to Figure 1, 4 and 5. Immunohistochemistry pictures of week 9 1st Trimester human fetal retina (A-I), DD28 LUMC0004iCTRL10 human iPSC-derived retinal organoids (J-P) and retinal organoids derived from hiPSC lines LUMC0080iCTRL12 (Q, R, S). Sections were stained with antibodies against: CRB1 and β-catenin (A-C), CRB2 and p120-catenin (D-F, D'-F'), PATJ and Ki67 (G-I) in week 9 human fetal retina. Sections were stained with antibodies against: CRB1 (J), CRB2 (K), PALS1 (L), MUPP1 (M), PATJ and Ki67 (N-P) in DD28-30 human iPSC-derived retinal organoids. Sections were stained with antibodies against: Recoverin and PAX6 (Q), CRB1 and β-catenin (R), CRB2 and p120-catenin (S) from retinal organoids derived from hiPSC lines LUMC0080iCTRL12. CRB1 was not found subapically of β-catenin (A-C) but CRB2 was found subapically of p120-catenin (D-F, D'-F') in week 9 human fetal retina. CRB2 was detected in week 9 fetal retinal pigment epithelium (D'-F'). PATJ was observed at the outer limiting membrane and also co-stained a subset of Ki67-positive cells (G-I, arrowheads) in week 9 human fetal retina. In DD28 human iPSC-derived retinal organoids CRB1 was not found at the subapical region (J) but CRB2 (K), PALS1 (L) and MUPP1 (M) were. PATJ also co-stained a subset of Ki67-positive cells in DD28 human iPSC-derived retinal organoids (N-P, arrowheads). Human iPSC lines LUMC0080iCTRL12 formed retinal organoids (Q). CRB1 was found subapically of β-catenin (R) and CRB2 was found subapically of p120-catenin (S). At least two independent differentiations/samples were analysed, 3-6 sections examined per organoid or fetal eye. RPE, retinal pigment epithelium; OLM, outer limitting membrane; NBL, neuroblast layer. Scale bars: 20μm (A-S).

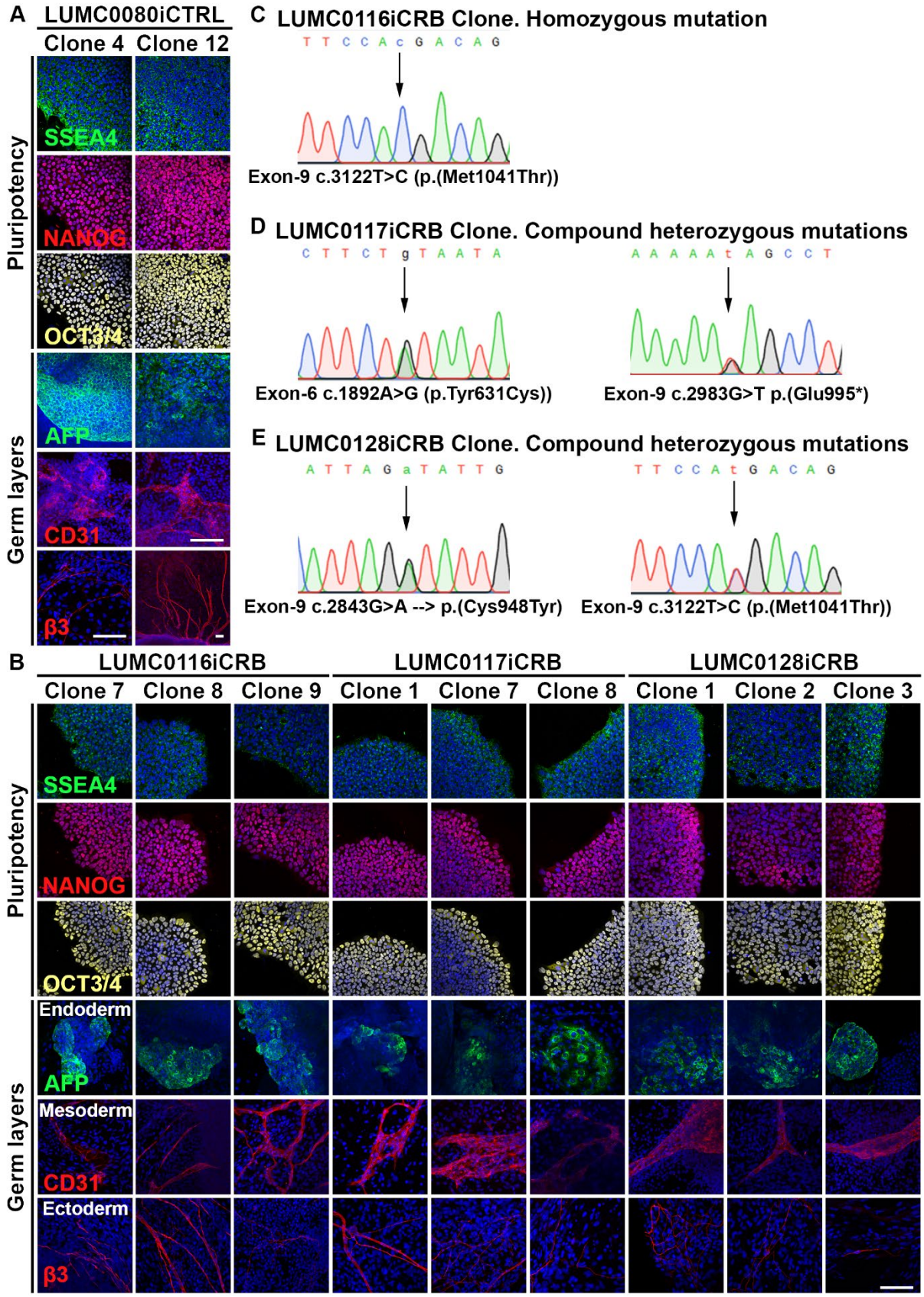
A
LUMC0080iCTRL
Clone 4
Clone 12
Pluripotency
SSEA4
NANOG
OCT3/4
Germ layers
AFP
CD31
β3
C
LUMC0116iCRB Clone. Homozygous mutation
T T C C A c G A C A G
Exon-9 c.3122T>C (p.(Met1041Thr))
D
LUMC0117iCRB Clone. Compound heterozygous mutations
C T T C T g T A A T A
Exon-6 c.1892A>G (p.Tyr631Cys))
A A A A A t A G C C T
Exon-9 c.2983G>T p.(Glu995*)
E
LUMC0128iCRB Clone. Compound heterozygous mutations
A T T A G a T A T T G
Exon-9 c.2843G>A --> p.(Cys948Tyr)
T T C C A t G A C A G
Exon-9 c.3122T>C (p.(Met1041Thr))
B
LUMC0116iCRB
LUMC0117iCRB
LUMC0128iCRB
Clone 7
Clone 8
Clone 9
Clone 1
Clone 7
Clone 8
Clone 1
Clone 2
Clone 3
Pluripotency
SSEA4
NANOG
OCT3/4
Germ layers
Endoderm
AFP
Mesoderm
CD31
Ectoderm
β3

Figure S4. Generation of human iPSC lines of *CRB1*-related retinitis pigmentosa patients. Related to Figures 4 and 5. Immunohistochemistry pictures of the characterization and validation of human iPSCs for pluripotency (SSEA4, NANOG, OCT3/4) and germ layers (AFP, CD31, β3). LUMC0080iCTRL clones 4 and 12 (A); LUMC0080iCTRL clones 4 and 12 (A); LUMC0116iCRB clones 7, 8, 9 (B); LUMC0117iCRB clones 1, 7, 8 (B); LUMC0128iCRB clones 1, 2, 3 (B). *CRB1* gene exon 6 and 9 was forward and reverse Sanger sequenced for patient lines (LUMC0116iCRB09, C; LUMC0117iCRB01, D; LUMC0128iCRB01, E) and healthy line LUMC0004iCTRL10 (not shown). The mutation in LUMC0116iCRB09 was validated as c.3122T>C (Effect: p(Met1041Thr)) (C). The mutations in LUMC0117iCRB01 was validated as heterozygous mutations with allele 1 being c.1892A>G (Effect: p.Tyr631Cys) and allele 2 being c.2983G>T (Effect: p.(Glu995*) (D). The mutations in LUMC0128iCRB01 was validated as heterozygous mutations with allele 1 being c.2843G>A (Effect: p.(Cys948Tyr) and allele 2 being c.3122T>C (Effect: p(Met1041Thr)) (E). All Scale Bars: 20 μm.

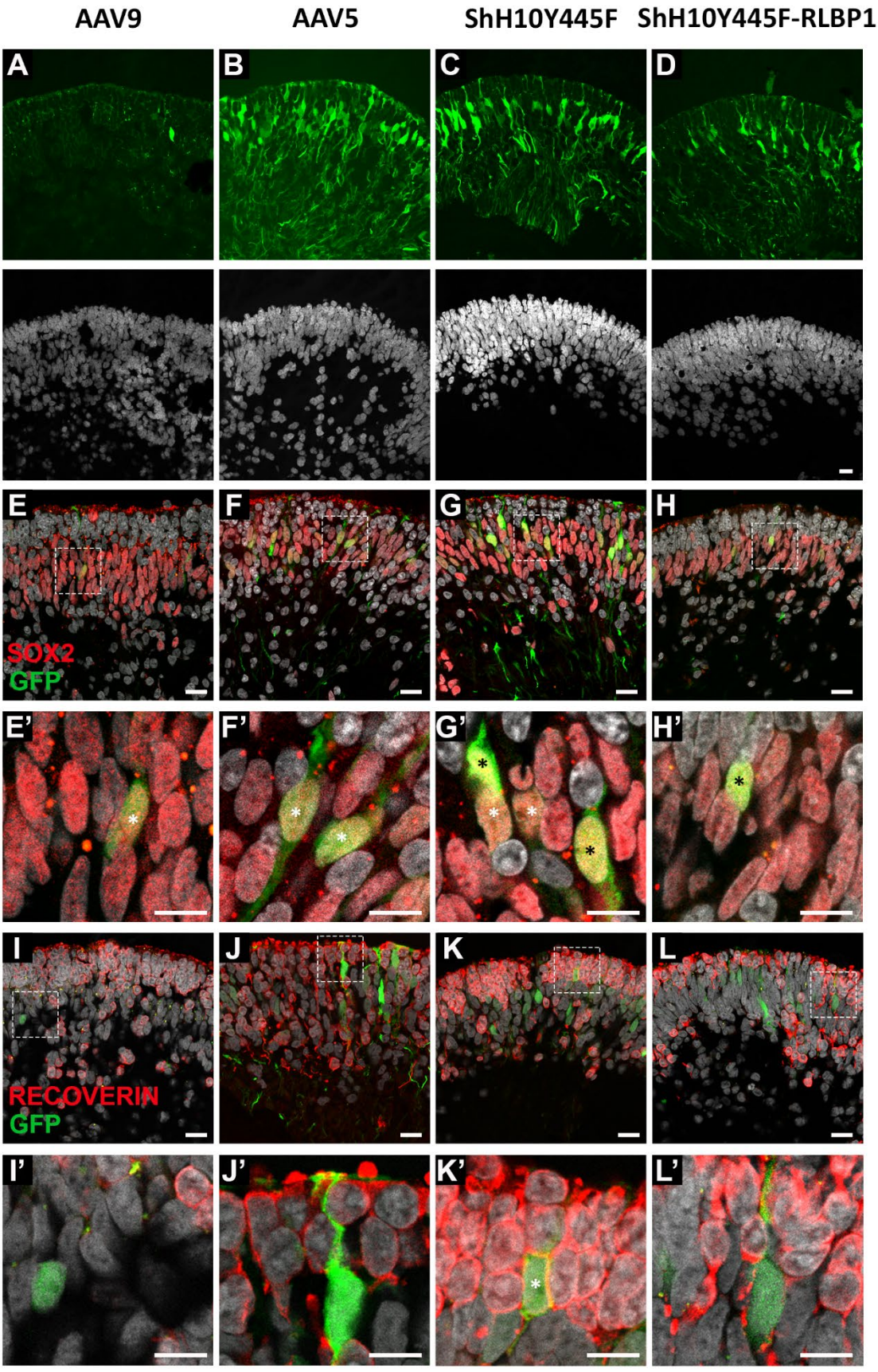
AAV9
AAV5
ShH10Y445F
ShH10Y445F-RLBP1
A
B
C
D
E
F
G
H
SOX2
GFP
E'
F'
G'
H'
I
J
K
L
RECOVERIN
GFP
I'
J'
K'
L'

Figure S5. AAV9, AAV5 and ShH10Y445F infect Müller glial cells. Related to Figure 5. Infection of 7.5 month old LUMC0004iCTRL10 human iPSC-derived retinal organoids at 10^{10}gc with AAV9-CMV-*GFP* (A, E, E', I, I'), AAV5-CMV-*GFP* (B, F, F', J, J'), ShH10Y445F-CMV-*GFP* (C, G, G', K, K') and ShH10Y445F-RLBP1-*GFP* (D, H, H', L, L'). High laser intensity images of AAV9- (A), AAV5- (B), ShH10Y445F-CMV-*GFP* (C) and ShH10Y445F-RLBP1-*GFP* (D). Infection with AAV9- CMV-*GFP*, AAV5- CMV-*GFP*, ShH10Y445F-CMV-*GFP* and ShH10Y445F-RLBP1-*GFP* showed co-staining with Müller glial marker SOX2 (E, F, G, H and inserts E', F', G', H') but not with photoreceptor marker Recoverin (I, J, K, L and inserts I', J', L'). Occasional GFP/recoverin-positive cells were detected (K'). Two independent differentiations of the hiPSC line LUMC0004iCTRL10 were used, 3-6 sections examined per organoid. Scale Bars: 20 μm (A-L), inserts 10 μm (E'-L').

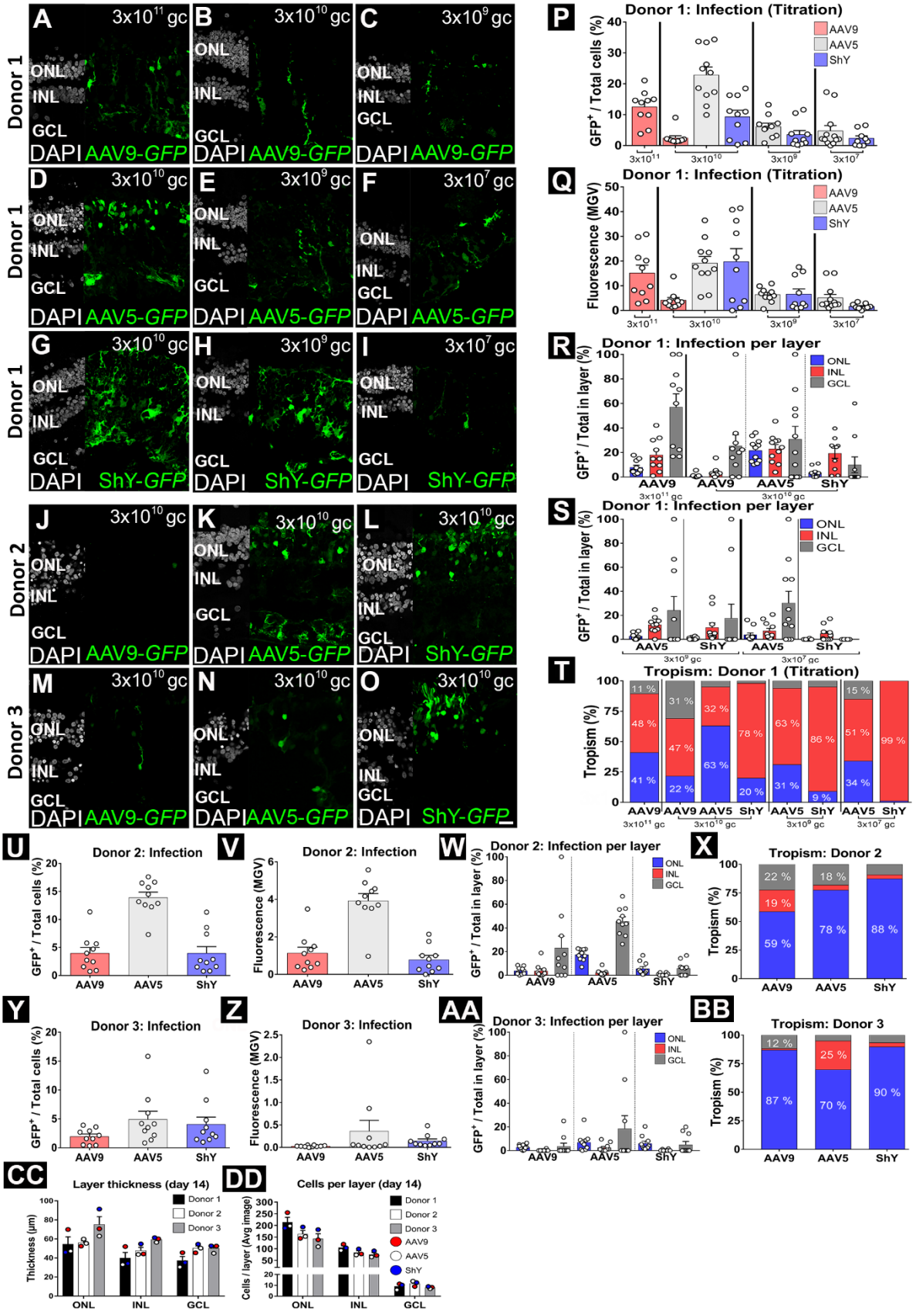
A
3x10^11 gc
B
3x10^10 gc
C
3x10^9 gc
Donor 1
ONL
INL
GCL
DAPI AAV9-GFP
D
3x10^10 gc
E
3x10^9 gc
F
3x10^7 gc
DAPI AAV5-GFP
G
3x10^10 gc
H
3x10^9 gc
I
3x10^7 gc
DAPI ShY-GFP
Donor 2
J
3x10^10 gc
K
3x10^10 gc
L
3x10^10 gc
Donor 3
M
3x10^10 gc
N
3x10^10 gc
O
3x10^10 gc
P
Donor 1: Infection (Titration)
GFP+ / Total cells (%)
AAV9
AAV5
ShY
Q
Donor 1: Infection (Titration)
Fluorescence (MGV)
R
Donor 1: Infection per layer
GFP+ / Total in layer (%)
S
Donor 1: Infection per layer
T
Tropism: Donor 1 (Titration)
Tropism (%)
11 %
48 %
41 %
31 %
47 %
22 %
32 %
63 %
78 %
20 %
63 %
31 %
86 %
9 %
15 %
51 %
34 %
99 %
U
Donor 2: Infection
V
Donor 2: Infection
W
Donor 2: Infection per layer
X
Tropism: Donor 2
22 %
19 %
59 %
18 %
78 %
88 %
Y
Donor 3: Infection
Z
Donor 3: Infection
AA
Donor 3: Infection per layer
BB
Tropism: Donor 3
12 %
87 %
25 %
70 %
90 %
CC
Layer thickness (day 14)
Thickness (µm)
ONL
INL
GCL
Donor 1
Donor 2
Donor 3
DD
Cells per layer (day 14)
Cells / layer (Avg image)
AAV9
AAV5
ShY

Figure S6. Titration of AAV serotypes on human donor 1 retina and independent repeats on donor 2 and 3. Related to Figure 6. Transduction of AAV9- (A-C, J, M), AAV5- (D-F, K, N) and ShH10Y445F (G-I, L, O) on human adult donor retina at $3x10^{11}$ gc (A), $3x10^{10}$ gc (B, D, G, J-O), $3x10^{9}$ gc (C, E, H), $3x10^{7}$ gc (F, I). AAV infection by total GFP-positive cells / Total cells infected for donor 1 (P). Infection measured by GFP-fluorescence for donor 1 (Q). GFP-positive cells per total cells in layer for donor 1 (R, S). Tropism: GFP-positive cells in layer per Total GFP-positive cells for donor 1 (T). Human adult donor retina 2 (J-L) and 3 (M-O). AAV potency measured by total GFP-positive cells / Total cells infected for donor 2 (U) and 3 (Y). Infection measured by GFP-fluorescence for donor 2 (V) and 3 (Z). GFP-positive cells per total cells in layer for donor 2 & 3 (W, AA). Tropism (GFP-positive cells in layer per Total GFP-positive cells) for donor 2 and 3 (X, BB). Retinal thickness between donors 1-to-3 at day 14 in culture (CC). Cells per layer in averaged image (DD). Each dot represents an individual image (P-BB). 90 images analysed donor 1, 30 images analysed donors 2 and 3 (CC and DD). ShY, ShH10Y445F; ONL, outer nuclear layer; INL, inner nuclear layer; GCL, ganglion cell layer; gc, genome copies. Scale bar: 20µm (A-O). Data are presented as mean ± SEM.

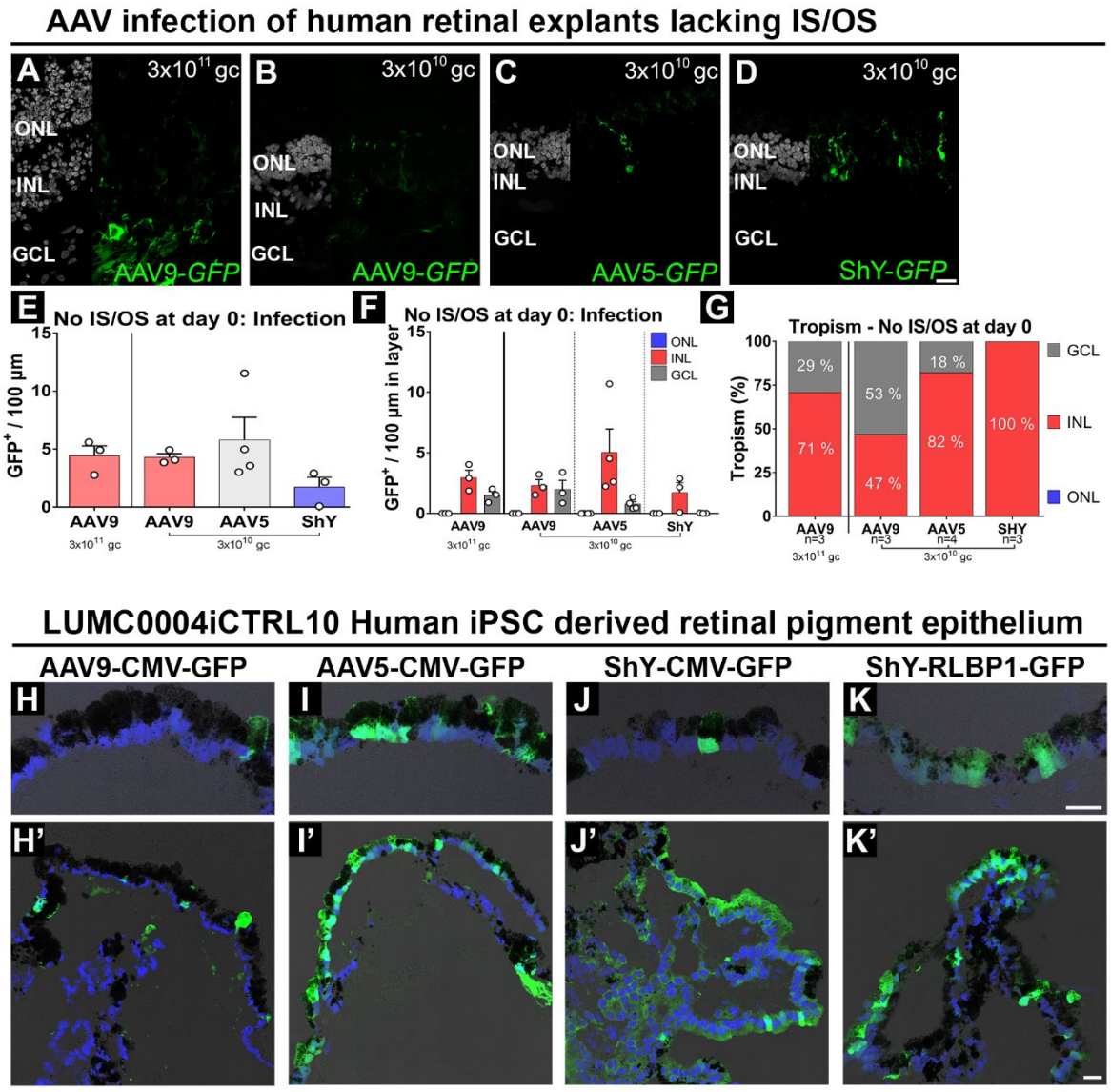

Figure S7. Human retinal explants lacking outer segments show no photoreceptor transduction. Related to Figure 6. Infection of human retinal explants missing outer segments with AAV9-CMV-*GFP* at $3x10^{11}$ gc (A) and $3x10^{10}$ gc (B), AAV5-CMV-*GFP* at $3x10^{10}$ gc (C) and ShH10Y445F-CMV-*GFP* at $3x10^{10}$ gc (D). Efficacy of transduction of retinal cell types was quantified by measuring the number of GFP-positive cells per 100 µm retinal length (E). GFP-positive cells per 100 µm retinal length in each layer (F). INL cells were mostly infected, and no photoreceptors were transduced by AAV9, AAV5 or ShH10Y445F (G). AAV9 at $3x10^{10}$ gc, $3x10^{11}$ gc and AAV5 at $3x10^{10}$ gc showed infection in the GCL. DAPI=grey. AAV-GFP=green. Each dot represents an individual donor (E, F), 10 images were analysed per donor (E-G). AAVs infect human iPSC derived retinal pigment epithelium. Related to Figure 7. LUMC0004iCTRL10 human derived retinal pigment epithelium is transduced at 10^{10} gc by AAV9-CMV-GFP (H, H'), AAV5-CMV-GFP (I, I'), ShH10Y445F-CMV-GFP (J, J') and ShH10Y445F-RLBP1-GFP (K, K'). DAPI=blue. Pigment=black. AAV-GFP=green. ShY, ShH10Y445F; ONL, outer nuclear layer; INL, inner nuclear layer; GCL, ganglion cell layer; gc, genome copies. Scale bar: (A-D, H-K, H'-K'), 20 µm. Data are presented as mean ± SEM.

Table S1. Antibody list and dilution used for immunohistochemistry and EM. Related to All Figures.

Antibody	Dilution	Manufacture	Catalogue Numbers
pH3	1:100	Millipore	06-570
Ki67	1:100	BD Biosciences	550609
p27kip1	1:200	Millipore	06-445
SOX9	1:250	Millipore	AB5535
Recoverin	1:500	Millipore	AB5585
Rhodopsin	1:500	Millipore	MAB5356
PAX6	1:100	DSHB	AB_528427
Islet1/2	1:200	DSHB	AB_2314683
Tuj1	1:200	Biolegend	801201
PKCα	1:250	BD Biosciences	610107
OTX2	1:200	Proteintech Europe	13497-1-AP
CRB1 AK2	1:200	Homemade	N/A
CRB2 EP13	1:200	gift from Pen Rashbass	N/A
CRB2 SK11	1:200	gift from Pen Rashbass	N/A
PALS1 SN47	1:200	Homemade	N/A
PAR3	1:100	Millipore	07-330
MUPP1	1:200	BD Biosciences	M98820
β-catenin	1:200	BD Biosciences	610153
p120-catenin	1:200	BD Biosciences	610134
N-Cadherin	1:250	BD Biosciences	610920
LHX2	1:200	Santa Cruz	sc-19344
peanut agglutinin (PNA)	1:200	Vector Lab	RL-1072
CD44	1:400	BD Biosciences	553132
PATJ	1:200	gift from André Le Bivic	N/A
SOX2	1:200	Santa Cruz	sc-17319
EAAT1 (GLAST)	1:100	Abcam	ab416
CRALBP	1:200	Abcam	ab15051
OPN1SW	1:200	Millipore	AB5407

Supplemental Experimental Procedures

Fetal human retinal tissue

Human fetal eyes at gestational age week 9 to 19 were collected from elective abortion material (vacuum aspiration) without medical indication, with signed informed consent and provided anonimised. In this study, "weeks of gestation" was used as determined by the last menstrual period (LMP).

Adult human retinal tissue

Patient anonymity was strictly maintained. All tissue samples were handled in a coded fashion, according to Dutch national ethical guidelines (Code for Proper Secondary Use of Human Tissue, Dutch Federation of Medical Scientific Societies). Post-mortem adult human donor eye (from 56 to 88 years-old donors) were acquired within the LUMC and were processed within 24 hours after death.

Cell Culture and Retinal Organoid Differentiation

Three healthy lines (LUMC0004iCTRL10, LUMC0044iCTRL44, LUMC0080iCTRL12) and three male *CRB1* RP patient lines (LUMC0116iCRB09, LUMC0117iCRB01, LUMC0128iCRB01) were derived from skin fibroblast using polycistronic Lentiviral vectors (Warlich et al., 2011). The *CRB1* RP patient line LUMC0117iCRB01 also had the variant c.1892A>G (p.(His631Arg)) in the *RPGRIP1* gene, which was classified as a variant of unknown significance.

In brief, human iPSCs were collected and incubated with (±)blebbistatin in mTeSR medium overnight and transitioned from mTeSR/NIM-1 (3:1), to (1:1), and to (0:1) over the subsequent three days to form Embryoid Bodies (EBs) in floating culture. Floating EBs were plated onto Matrigel-coated wells from differentiation day (DD) 7 till DD28, with a change from NIM-1 to NIM-2 medium at DD16. At DD28 neuroepithelial rosettes are flushed loose from the matrigel using a P1000 pipet and are kept in floating culture in agarose coated plates from this point onwards. NIM-2 is used till DD41, RLM is used from DD42 to DD48, RLM-1 from DD49 to DD97, and RLM-2 from DD98 for long-term culture. Medium is changed as required, typically every other day from DD3 till DD33 and typically twice a week from DD41 onwards. Plates were checked for possible medium changes every other day. Neural Induction Medium 1 (NIM-1): 48.95 mL DMEM/F12 supplemented with 0.5 mL 100x N2 supplement, 0.5 mL 100x Minimum Essential Media-Non Essential Amino Acids (MEM NEAAs), 10 µL 10 mg/mL Heparin (Sigma). Neuronal Induction Medium 2 (NIM-2): 96 mL DMEM/F12 (3:1) supplemented with 2 mL 50x B27 Supplement, 1 mL 100x NEAA, 1 mL 100x antibiotic-antimycotic (10,000 units/mL of penicillin, 10,000 µg/mL of streptomycin, 25 µg/mL of amphotericin B). Retinal Lamination Medium (RLM): 107.25 mL DMEM/F12 (3:1) supplemented with 12.5 mL embryonic stem cell-qualified FBS, 2.5 mL 50x B27 Supplement, 1.25 mL 100x MEM NEAAs,1.25 mL 100x antibiotic-antimycotic (10,000 units/mL of penicillin, 10,000 µg/mL of streptomycin, 25 µg/mL of Amphotericin B), 0.25 mL taurine (100 µM final concentration). Retinal Lamination Medium 1 (RLM-1): RLM supplemented with 0.1 µL 10 mM retinoic acid (1 µM final concentration) per mL. Retinal Lamination Medium 2 (RLM-2): RLM supplemented with 0.05 µL 10 mM retinoic acid (0.5 µM final concentration) per mL.

Sequence validation on patient mutations in the *CRB1* gene

DNA of retinal cells were extracted with the DNeasy Blood & Tissue Kit (QIAGEN) from *CRB1* RP patient retinal organoids (LUMC0116iCRB09, LUMC0117iCRB01, LUMC0128iCRB01). Exon 6 was PCR amplified (Forward primer: TTTGAGGGCGATGGCTTCCT. Reverse primer: TGAGGCATGGCACTCCTAGC). Exon 9 was PCR amplified (Forward primer: TGAACAAAATTACTTAAATTCTGTGAG. Reverse primer: TCCTCCATGCAAACAGGGGT). The samples were then purified (QIAquick PCR Purification) and then Sanger sequenced. Exon 6 was Sanger sequenced in forward and reverse direction (Forward primer: TAATCAGTCAAAGGTGCTTCTGTT. Reverse primer: CTCTCAGACAGTTGGGGCCT). Exon 9 was sequenced in forward and reverse direction (Forward primer: TGAACAAAATTACTTAAATTCTGTGAG. Reverse primer: TGTACTTAGACACCCTTGCAG). The electropherograms were analysed in Snapgene

Viewer (Version 3.2) and aligned to Exon 6 and Exon 9 extracted from the *CRB* gene region Chromosome 1: 197,268,278-197,478,455 (ENSG00000134376 GRCh38).

Immunohistochemical analysis

Adult human donor retina, human fetal retina, hiPSC-derived retinal organoids were incubated for 30 minutes in 4% paraformaldehyde in PBS for fixation and 15% and then 30% sucrose in PBS for cryo-protection. Finally, retina were orientated, embedded in Tissue-Tek, frozen and stored at -20°C. Sections of 8-10 µm were made with a Leica CM1900 cryostat (Leica Microsystems). Sections for immunohistochemistry were blocked for 1 hour in 10% normal goat serum, 0.4% Triton X-100 and 1% bovine serum albumin (BSA) in PBS, incubated in a moist-chamber overnight at 4°C (Table S1) diluted in 0.3% normal goat serum, 0.4%Triton X-100 and 1% BSA in PBS. After rinsing in PBS, the sections were incubated for 1 hour with complementary conjugated secondary antibodies (Table 1) and rinsed in PBS again. Sections were mounted in Vectashield HardSet DAPI mounting media (Vector Laboratories). A Leica TCS SP8 confocal microscope were used for Image acquisition. Image analysis and processing were carried out using ImageJ and Adobe Photoshop CC2014, respectively.

Electron microscopy

In brief, 40 µm thick sections were incubated with the appropriate first antibody for 48 h (Table 1), then incubated with appropriate secondary (anti-Rabbit or anti-Mouse) peroxidise anti-peroxidase (PAP) for 2h, then developed in a 2,2-diaminobenzidine solution containing 0.03% H_2O_2 for 4 min and then the gold substitute silver peroxidise method applied. Sections were embedded in epoxy resin, ultrathin sections made and examined with an electron microscope (Microscope: FEI Tecnai T12 Twin Fei Company, Eindhoven, The Netherlands; Camera: OneView, Gatan) operating at 120 kV. Overlapping images were collected and stitched together into separate images as previously described (Faas et al., 2012). At least two independent samples were analysed per time point for human fetal eyes and human iPSC-derived retinal organoids and RPE.

Generation and purification of the viral vectors

Briefly, pAAV2-*eGFP* plasmids were co-transfected with the pHelper and pAAV9, pXX2-ShH10Y445F, or pDP5rs capsid plasmid into HEK293T cells to generate AAV9, ShH10Y445F or AAV5 viral particles. After benzonase treatment, the lysates were ultra-centrifuged onto an iodixanol density gradient and concentrated on Amplicon spin columns (100 kDa, Millipore). All viral titers were determined by quantitative PCR and all viral stocks with titers around 1×10^{13} genome copies per ml were stored at −80°C.

In vitro transduction of human donor retina and human induced pluripotent stem cell derived retinal organoids

1) In brief, 3-6 6 mm punches of human donor retina were dissected in cold HBSS (Sigma) within 24 hours after death. Whatman™ paper was placed on the ganglion cell side of each punch. Punches were then placed, photoreceptor side down, on Millicell Cell culture Inserts (Millipore, PICM01250) and placed into a 24 well plate with 300 µL of explant medium per well. After that, 50 µL of explant medium with the desired titre of a viral vector ($3x10^7$, $3x10^9$, $3x10^{10}$ or $3x10^{11}$ gc) was added to Whatman™ paper for 48 hours, and medium changed every other day until day 14. Explant medium: 300 µL 50X B-27 Supplement (Invitrogen), 150 µL 100X N-2 Supplement (Invitrogen), 30 µL 50 mM Taurine, 120 µL 200 mM L-glutamine, 150 µL 100 mM sodium pyruvate, 18.45 µL 1 mM N-Acetyl-L-cysteine, 150 µL 100X antibiotic-antimycotic (10,000 units/mL penicillin, 10,000 µg/mL streptomycin, 25 µg/mL Amphotericin B) in a final volume of 15 mL Neurobasal®-A medium (Invitrogen). 2) In brief, two retinal organoids were placed in 1%-agarose coated wells of a 96-well plate, and 50 µl of RLM-2 containing the 10^{10} gc of the AAV vector was added for 24 hours. A further 50 µL of RLM-2 only was added to the well for another 24 hours. The organoids were washed three times in PBS and replated in RLM-2 in a 24-well plate. The medium was then changed twice a week for 14 days post infection. Tissues were fixed, cryo-protected and frozen for further processing as described in: Immunohistochemical analysis.

Quantitative analysis of GFP fluorescence intensity and cell number

Quantitative analysis of GFP expression allowed for assessment of both AAV potency and tropism in human donor retina and hiPSC-derived retinal organoids. For the quantitative analysis of GFP expression, images were taken using a Leica TCS SP8 confocal microscope (Leica). Images were obtained at 40x magnification using identical acquisition settings, including laser intensity, and were saved at a resolution of 1024x1024 pixels. GFP expression profiles were measure in three ways: 1) GFP positive cells per total cells, 2) Mean grey value (Transduction profiles were analyzed by defining a region of interest (ROI) for the outer nuclear layer, inner nuclear layer and ganglion cell layer for human donor material and a top nuclear layer and bottom nuclear layer for the hiPSC-derived retinal organoids), and 3) GFP-positive cells in layer per cells in layer. Tropism was measured as GFP-positive cells in layer (ONL, INL or GCL/Nerve Fiber Layer) per total GFP-positive cells. The Cell Counter plugin for ImageJ was used to quantify total cell number (counterstain: DAPI, LHX2, and SOX2) and total GFP positive cell number for each ROI. The number of GFP positive cells for each ROI was divided by the total number of cells for each ROI to obtain the percentage of transduced cells. Fluorescence images were also analysed by calculating the mean grey value (MGV), corrected for area and background levels of fluorescence, for each ROI using ImageJ software. 6-mm harvested retinal explant punches were sectioned at 90 degree angle (Buck et al., 2018). This allows to assess the AAV transfection on the whole retina stretch of 6-mm retinal explant punch. Edges or otherwise damaged areas where not used for image acquisition. Between 3-6 different sections from at least three different human donor retina or hiPSC-derived retinal organoids were used for quantification of mean grey value or cell counting's (>900 μm in retinal length. 3-5 images per organoid and 10 images for adult donor retina).

Supplemental References

Buck, T.M., Pellissier, L.P., Vos, R.M., van Dijk, E.H.C., Boon, C.J.F., and Wijnholds, J. (2018). AAV Serotype Testing on Cultured Human Donor Retinal Explants. Methods Mol. Biol. *1715*, 275–288.
Faas, F.G.A., Cristina Avramut, M., van den Berg, B.M., Mieke Mommaas, A., Koster, A.J., and Ravelli, R.B.G. (2012). Virtual nanoscopy: Generation of ultra-large high resolution electron microscopy maps. J. Cell Biol. *198*, 457–469.
Warlich, E., Kuehle, J., Cantz, T., Brugman, M.H., Maetzig, T., Galla, M., Filipczyk, A.A., Halle, S., Klump, H., Schöler, H.R., et al. (2011). Lentiviral vector design and imaging approaches to visualize the early stages of cellular reprogramming. Mol. Ther. *19*, 782–789.